



This open access document is published as a preprint in the Beilstein Archives with doi: 10.3762/bxiv.2020.78.v1 and is considered to be an early communication for feedback before peer review. Before citing this document, please check if a final, peer-reviewed version has been published in the Beilstein Journal of Nanotechnology.

This document is not formatted, has not undergone copyediting or typesetting, and may contain errors, unsubstantiated scientific claims or preliminary data.

**Preprint Title** Out-of-plane surface patterning by subsurface processing of polymer substrates with focused ion beams

**Authors** Serguei Chiriaev, Luciana Tavares, Vadzim Adashkevich, Arkadiusz J. Goszczak and Horst-Guenter Rubahn

**Publication Date** 30 Jun 2020

**Article Type** Full Research Paper

**ORCID® IDs** Serguei Chiriaev - <https://orcid.org/0000-0001-8274-9864>; Luciana Tavares - <https://orcid.org/0000-0002-1432-524X>; Arkadiusz J. Goszczak - <https://orcid.org/0000-0002-1731-4781>; Horst-Guenter Rubahn - <https://orcid.org/0000-0002-3606-5653>

# Out-of-plane surface patterning by subsurface processing of polymer substrates with focused ion beams

Serguei Chiriaev\*<sup>1</sup>, Luciana Tavares<sup>1</sup>, Vadzim Adashkevich<sup>2</sup>, Arkadiusz J. Goszczak<sup>1</sup> and Horst-Günter Rubahn<sup>1</sup>

<sup>1</sup>NanoSYD, Mads Clausen Institute, University of Southern Denmark, Alsion 2, Sønderborg, 6400, Denmark and <sup>2</sup>Centre for Industrial Electronics, Mads Clausen Institute, University of Southern Denmark, Alsion 2, Sønderborg, 6400, Denmark

E-mail:

Serguei Chiriaev\* - [schi@mci.sdu.dk](mailto:schi@mci.sdu.dk)

\*Corresponding author

Keywords: focused helium ion beam; polymers; thin films; out-of-plane nanopatterning; direct patterning

## Abstract

This work explores a new technique for the out-of-plane patterning of nanostructures prefabricated on the surface of a polymer substrate. The technique is based on ion-beam-induced material modification in the bulk of a polymer. Effects of subsurface and surface processes on the surface morphology have been studied for three polymer materials (Polymethylmethacrylate, Polycarbonate and Polydimethylsiloxane) by using irradiations with He<sup>+</sup>, Ne<sup>+</sup> and Ga<sup>+</sup> focused ion beams. Thin films of a Pt<sub>60</sub>Pd<sub>40</sub>-alloy and of pristine Au were used to mimic nanostructured thin films. We show that the height of thin Pt<sub>60</sub>Pd<sub>40</sub> films deposited on Polymethylmethacrylate and Polycarbonate substrates can be patterned by He<sup>+</sup> ion beam with nanometer precision while preserving nanometric features of the pre-deposited films. Ion irradiation of the Au-coated samples results in Au-film delamination, bulging and perforation, which is attributed to accumulation of radiolysis gases at the film-substrate interface. The irradiation with Ne<sup>+</sup> and Ga<sup>+</sup> ions destroys the films and roughens the surface due to dominating sputtering processes. A very different behavior, resulting in the formation of complex, multiscale 3D- patterns, is observed for Polydimethylsiloxane samples. The roles of the metal film structure, elastic properties of the polymer substrate and irradiation-induced mechanical strain in the patterning process are elaborated and discussed.

## Introduction

Micro and nanofabrication with focused ion beams (FIBs) is at present of strong interest within diverse fields of materials science and technology [1]. The capabilities of FIBs have in recent years been substantially enhanced for a broad range of applications by implementation of light-mass ion beams (He<sup>+</sup> and Ne<sup>+</sup>) emitted by a gas field ion source (GFIS). This has enabled direct, mask-less surface patterning with a superior lateral resolution and depth control [2, 3]. The portfolio of the

currently used FIB-based and FIB-assisted surface patterning techniques includes a number of different methods, such as ion-beam sputtering of surface layers (ion-beam-milling), ion-beam assisted chemical etching and ion-beam assisted chemical vapor deposition [1-3]. All these methods are based on processes of either adding or removing atoms on the surface or in the subsurface atomic layers.

It is also well known that the ion beams deposit their energy and therefore affect structure and properties of materials over the entire depth of their penetration in a target. In our recent work [4], we have demonstrated, that in addition to the direct surface patterning by the abovementioned techniques, the radiation damage generated by  $\text{He}^+$  FIB in the bulk of Polymethylmethacrylate (PMMA) substrates can be used for well-controlled and nanometer-precise patterning of the height of thin metal films and nanostructures prefabricated on the surface of these substrates. The technique is based on subsurface chemical decomposition, structural reconstruction, and as a result of these processes, volume shrinkage of PMMA polymer under ion irradiation [5-7]. The most important physical and chemical phenomena behind this material modification include polymer-chain scission and cross-linking, which can occur simultaneously, formation of volatile molecules and their desorption from the polymer bulk [7]. In fact, the method utilizes ion energy losses to manipulate the surface morphology by means of radiation damage generated in the substrate bulk and minimizes the surface damage resulted from sputtering. This leaves the thin films and thin-film nanostructures prefabricated on the PMMA surface essentially intact and provides a new route to their out-of-plane patterning, which is interesting for a range of thin film applications.

In the current work, we extend our study to the effects of ion masses, by irradiating PMMA substrates with  $\text{He}^+$ ,  $\text{Ne}^+$  and  $\text{Ga}^+$  ions, and to the role of pathways for volatile radiolysis products to escape the irradiated material. We also investigate the possibility to pattern a surface by subsurface substrate processing with  $\text{He}^+$  ions for other polymer substrates, such as polycarbonate (PC) and polydimethylsiloxane (PDMS). The choice of materials for this work has been directed by their diverse applications in micro and nanotechnology, and by the high susceptibility of their structure to ion irradiation (see e.g. Ref. 5 and references therein). Another important aspect is that the chosen materials are different in their structure, chemical composition and mechanical properties. This provides an appropriate playground for a comparative study of the role of material-related factors in the FIB-induced surface patterning. PMMA and PC polymers are especially interesting for many reasons: PMMA is widely used as a positive resist for X-ray, deep UV [8], electron and ion-beam lithography [9]. Structural transformation and volume shrinkage of PMMA under ion irradiation have been reported in a large number of publications (e.g. [6, 7, 9-13]). PC is the second largest sales-volume thermoplastic polymer. It is extensively used in microtechnology due to its excellent optical, mechanical, and chemical properties [14]. Compared to PMMA, it has much higher mechanical toughness, thermal resistance, chemical stability, and as PMMA, is widely used in optical applications. A range of publications show that, owing to its radiation susceptibility, PC can be used as a positive or negative resist for

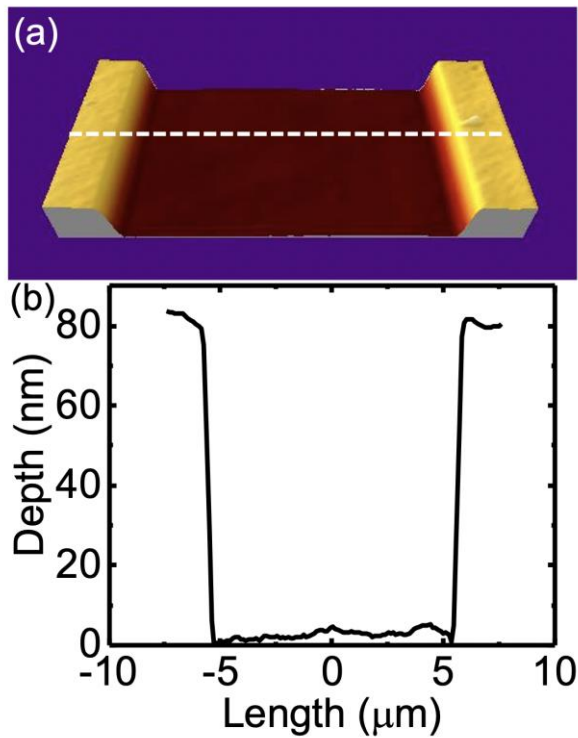
electron beam lithography [15, 16]. It has been also demonstrated that it performs as a kind of ion-beam-resist in fabrication of micro- and nanopore membranes and templates for nanowires by chemical etching of through-holes along ion tracks produced by high energy ions [17,18].

In contrast to PMMA and PC polymers, PDMS is a mineral-organic polymer (its structure includes both carbon and silicon atoms), and it is an elastomer, the elasticity of which can be tuned within a very large range by changing the degree and the type of polymerization, and by post-curing treatments [19, 20]. The high and easy-tunable elasticity, combined with high transparency, biocompatibility and low cost, provides a broad use of PDMS in fabrication of microfluidic, micro-electro-mechanical and micro-optical devices [20]. The effects of ion irradiation on chemical and physical properties, and the surface morphology of PDMS, have been investigated in a vast amount of research (see e.g. Ref [21 - 24] and references therein). The observed phenomena, most important for the goals of this study, can be summarized as follows: i) ion beam irradiation can result in a significant compacting, and at some conditions, in swelling of the irradiated PDMS areas [25], ii) a stiff “skin” layer produced by ion irradiation on the PDMS surface leads to formation of ordered wrinkle-like micropatterns [23, 24].

## Results and discussion

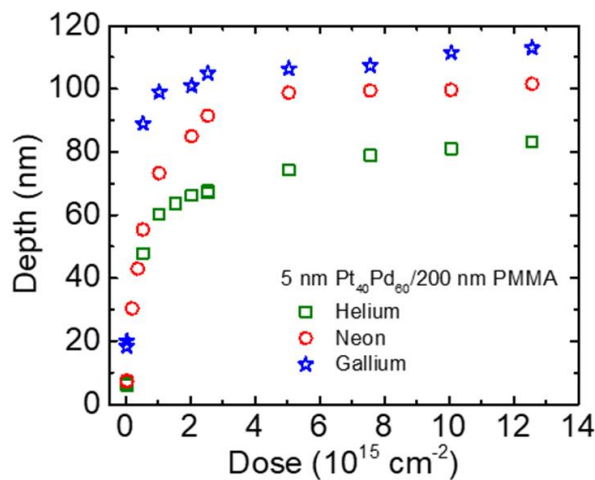
### Irradiation of PMMA

Figure 1 shows an example of an AFM image and the corresponding depth profile for a surface region of the Pt<sub>60</sub>Pd<sub>40</sub>/ PMMA sample irradiated with He<sup>+</sup> FIB to a dose of  $1.0 \times 10^{16} \text{ cm}^{-2}$ . It is well seen that the irradiation draws the entire irradiated surface homogeneously down to a depth of about 80 nm. For convenience, we define the value of the surface depression as a reduction in the surface height (or as a change in the surface depth), for which the baseline values correspond to the non-irradiated area. Patterns of similar shape have been observed for the entire dose range of the irradiation with He<sup>+</sup> ions, and for the irradiations with Ne<sup>+</sup> and Ga<sup>+</sup> ions as well.



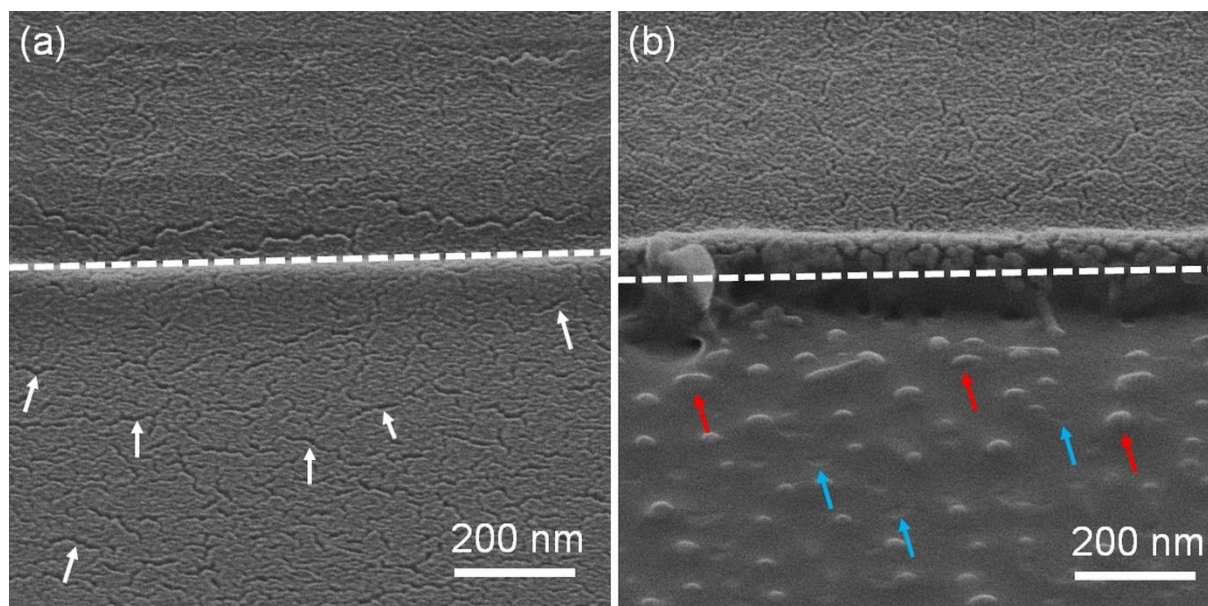
**Figure 1:** An AFM image (a) and the corresponding depth profile (b) of a fragment of the surface depression produced in a 5 nm Pt<sub>60</sub>Pd<sub>40</sub> / 200nm PMMA sample, by irradiation with He<sup>+</sup> FIB at an energy of 25 keV to a dose of  $1.0 \times 10^{16}$  cm<sup>-2</sup>. Dashed line in a) indicates the place of the depth profile.

Figure 2 summarizes the dependence of the surface deepening as a function of irradiation dose for He<sup>+</sup>, Ne<sup>+</sup> and Ga<sup>+</sup> ions. All curves demonstrate very steep increase in depth with increasing dose at low doses, followed by saturation when the doses become higher. The influence of ion type on the surface depth is apparent from the comparison of these plots: Both the depth change rate at low doses, and the depth saturation level increase with an increase in the ion mass.



**Figure 2:** Dose dependencies of the irradiation induced surface deepening for a 5 nm Pt<sub>60</sub>Pd<sub>40</sub> / 200nm PMMA sample, irradiated with 25 keV He<sup>+</sup>, Ne<sup>+</sup> and Ga<sup>+</sup> FIBs.

Figure 3 compares surface morphology of 5 nm Pt<sub>60</sub>Pd<sub>40</sub> / 200 nm PMMA samples in the case of a high dose irradiation with He<sup>+</sup> and Ga<sup>+</sup> ions. The metal film has survived the irradiation with He<sup>+</sup> ions but it is extinct by the Ga<sup>+</sup> ion irradiation. Besides, the Ga<sup>+</sup> irradiated area is much rougher and characterized by erosions and spot-like elevations. For an irradiation dose of  $2.0 \times 10^{15} \text{ cm}^{-2}$  for instance, the values of root mean square (RMS) roughness, measured with AFM in the irradiated areas, were about 0.7 nm and 4.4 nm for the He<sup>+</sup> and Ga<sup>+</sup> irradiations, respectively. The RMS roughness value of the pristine sample was about 0.6 nm. The irradiation with Ne<sup>+</sup> ions also roughens the surface significantly and sputters away the metal film. The RMS roughness was about 3.1 nm after the irradiation with Ne<sup>+</sup> FIB to a dose of  $2.0 \times 10^{15} \text{ cm}^{-2}$ .



**Figure 3:** HIM images of a 5 nm Pt<sub>60</sub>Pd<sub>40</sub> / 200nm PMMA sample irradiated to a dose of  $1.2 \times 10^{16} \text{ cm}^{-2}$  with He<sup>+</sup> (a) and Ga<sup>+</sup> FIB (b). In (a) and (b), dashed lines indicate the border between the irradiated (the lower parts) and non-irradiated (the upper parts) regions. White arrows in a) indicate some of the nano-cracks. In b), red and blue arrows indicate the local surface elevations and erosions, respectively.

It is well known that the sputtering efficiency of Ga<sup>+</sup> and Ne<sup>+</sup> ions is substantially higher than that of He<sup>+</sup> ions [3], due to the much larger masses of Ne<sup>+</sup> and Ga<sup>+</sup> ions (20 and 70 AMU, respectively) as compared to 4 AMU for He<sup>+</sup> ions. The above results provide thus a direct experimental confirmation of in-applicability of middle and heavy mass ions in the scope of our nanopatterning technique, because they destroy the virgin surface morphology and sputter away the pre-deposited films.

The observed increase in the surface descending rates and the saturation level in the case of irradiation with Ne<sup>+</sup> and Ga<sup>+</sup> ions (Figure 2) indicate that in those cases both surface sputtering and subsurface volume shrinkage contribute to the depth changes. To consider this in detail we first recall the results and discussion of our previous study [4], which showed that the reduction in surface height of the metal coated PMMA surface is controlled by two major parameters. The first is the

irradiation dose of  $\text{He}^+$  ions, which determines the total amount of radiation energy dissipated by the ions over their entire path in the sample. The second parameter is the thickness of the polymer layer, which determines the fraction of this total energy dissipated specifically in the polymer layer. An additional and important aspect is that the polymer materials cannot shrink infinitely with an increase in the irradiation dose, and at a certain dose, the material capacity to shrink becomes depleted, which explains the saturation effect. In PMMA particularly, the high irradiation doses result in the formation of a compact carbon-rich material [13], for which shrinkage is not longer possible. Taking this into consideration, we assume that a combination of several factors is responsible for the enhanced reduction in the surface height by  $\text{Ne}^+$  and  $\text{Ga}^+$  ions, compared to the irradiation with  $\text{He}^+$  ions.

The first factor is that the heavier ions deposit a larger fraction of energy in the PMMA layer, which is illustrated by energy loss profiles simulated with the SRIM software ('The Stopping and Range of Ions in Matter') as shown in Figure S1 in the supplementary material: In the case of  $\text{He}^+$  ion irradiation, a significant fraction of the total ion energy is lost in the silicon substrate below the PMMA layer (Figure S1a and b), meaning that this fraction is wasted from the point view of defect generation inside the PMMA layer. In contrast,  $\text{Ne}^+$  and  $\text{Ga}^+$  ions lose their energy entirely in the PMMA, and therefore, the total ion energy is utilized for defect generation in this layer (Figure S1c, d, e and f).

The second important factor includes the simultaneous contribution of ion sputtering as well as compacting and carbonization processes near the surface, which are significantly more effective in the case of irradiation with the middle and large mass ions, due to the much large density of ion energy deposited near the surface in nuclear collisions. The importance of the carbonization and compacting in the surface sputtering process has been demonstrated in [13].

Figure 4 outlines our results for PMMA samples coated with a 15 nm thick Au film and irradiated with 25 keV/ $\text{He}^+$  FIB. In contrast to the results obtained for the samples coated with  $\text{Pt}_{60}\text{P}_{40}$  films, extensive delamination and bulging of the Au film from the substrate surface are observed in the irradiated cells and in the regions surrounding the cells. This is well seen as changes in the color contrast in the cells of rows 1 and 2 in Figure 4a and confirmed by AFM imaging (Figure 4b). These effects are attributed to accumulation of radiolysis gases at the Au-film/PMMA interface, the pressure of which becomes at a certain dose and at certain places high enough to delaminate and bulge the film. At higher doses (corresponding to the cells in row 3, Figure 4a), the bulges are almost vanished, which can be explained by an appearance of holes in the irradiated regions (such as e. g. in cells **A3** and **B3**, Figure 4a), which provides gas release and deflation of the bulges. The above results demonstrate the important role of pathways for desorption of radiolysis gases. Moreover, our study shows that thin Au films (in our case, 15 nm thick) appear to be very strong barriers for permeation of gases and can withstand high degrees of stretching required for the observed bulging. Another remarkable result is the bulging outside the irradiated areas (see, e.g., Figure 4b), which we consider as a result of bulge nucleation at the boundary between the irradiated and non-irradiated regions, followed by in-plane bulge propagation inside and outside the irradiated regions.

From a technological point of view, the above results show that continuous and low-permeable films are not applicable for the overall technology suggested in this article. However, such films can be utilized in other forms: A gas leakage path, such as an array of micro-holes for instance, can be intentionally prefabricated in the films before irradiation, or instead of a continuous film, an array of discrete film features can be pre-deposited on the substrate.

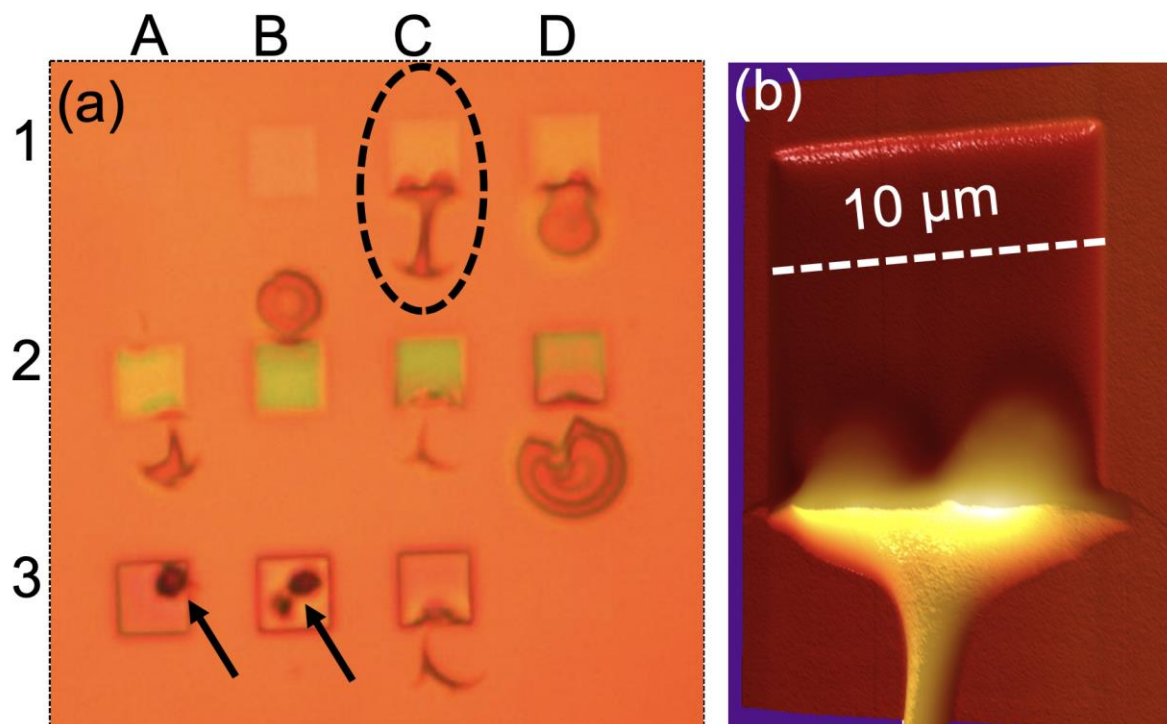


**Figure: 4.** a) Optical micrograph of an array of squares produced with He<sup>+</sup>/25 keV FIB in a 15 nm Au / 200 nm PMMA sample. The irradiation dose increases in a raster scan order as follows: **A1** ( $3.3 \times 10^{13} \text{ cm}^{-2}$ ), **B1** ( $2.0 \times 10^{14} \text{ cm}^{-2}$ ), **C1** ( $3.7 \times 10^{14} \text{ cm}^{-2}$ ), **D1** ( $5.3 \times 10^{14} \text{ cm}^{-2}$ ), **A2** ( $1.0 \times 10^{15} \text{ cm}^{-2}$ ), **B2** ( $2.0 \times 10^{15} \text{ cm}^{-2}$ ), **C2** ( $2.5 \times 10^{15} \text{ cm}^{-2}$ ), **D2** ( $5.1 \times 10^{15} \text{ cm}^{-2}$ ), **A3** ( $7.6 \times 10^{15} \text{ cm}^{-2}$ ), **B3** ( $1.0 \times 10^{16} \text{ cm}^{-2}$ ), **C3** ( $1.3 \times 10^{16} \text{ cm}^{-2}$ ), **D3** ( $3.3 \times 10^{13} \text{ cm}^{-2}$ ). The lowest dose ( $3.3 \times 10^{13} \text{ cm}^{-2}$ ) was irradiated in cells **A1** and **D3** to control the reproducibility of the obtained results. b) an AFM image of square **C1**.

### Irradiation of PC

The results of irradiation with He<sup>+</sup> FIB for 15 nm Pt<sub>60</sub>Pd<sub>40</sub> / PC samples appear to be similar to those obtained for the 15 nm Pt<sub>60</sub>Pd<sub>40</sub> / PMMA samples: AFM images and corresponding depth profiles (an example is presented in Figure 5a) show that within the entire dose range He<sup>+</sup> FIB irradiation draws the surface uniformly down. High magnification HIM images (e.g. Figure 5b) demonstrate preservation of the metal film and the presence of cracks in the irradiated and non-irradiated areas of this film.

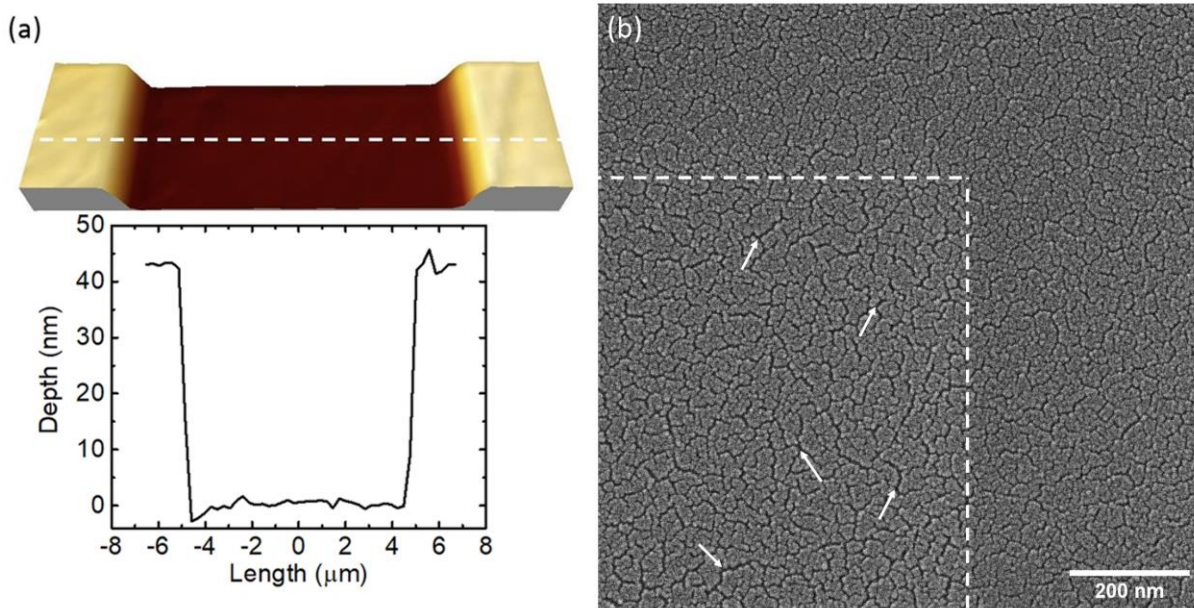


**Figure 5:** An AFM image and a corresponding depth profile (a) of a part of the surface depression produced in a 15 nm Pt<sub>60</sub>Pd<sub>40</sub> / PC sample by irradiation with He<sup>+</sup> FIB at an energy of 25 keV to a dose of  $2.0 \times 10^{15} \text{ cm}^{-2}$ . Dashed line in a) indicates the place of the depth profile. b) HIM image of a part of the same depression, demonstrating the persistence of metal film. White arrows mark some of the nano-cracks in the Pt<sub>60</sub>Pd<sub>40</sub> film in the irradiated region. Dashed lines indicate the border between the irradiated and non-irradiated regions.

The dependence of the surface descending depth on the irradiation dose for the 15 nm Pt<sub>60</sub>Pd<sub>40</sub> / PC sample is shown in Figure 6 and compared to the dose dependence for a 15nm Pt<sub>60</sub>Pd<sub>40</sub> / 770 nm PMMA sample obtained in our previous work [4]. The shapes of the curves are similar. The depth change rate and the absolute values as function of dose, however, are significantly lower in the case of PC substrates, and as a result, the total depth change observed at the highest dose ( $7.5 \times 10^{15} \text{ cm}^{-2}$ ) is about 2.5 times smaller than that in the case of the PMMA substrate. This difference can be a result of a combination of several factors related to the polymer structure and composition, as well as to the structural response of these materials to irradiation. This requires a more extended study. As far as the subject of this article is concerned, we conclude that the PC material is applicable for the suggested patterning scheme similar to PMMA. Higher rates and values of the surface height reduction can be achieved by increasing the ion energy. The above results are consistent with previous reports on chain scission, cross-linking and material compacting under exposure to different types of electromagnetic and corpuscular radiation (e.g. [26, 27] and references therein).

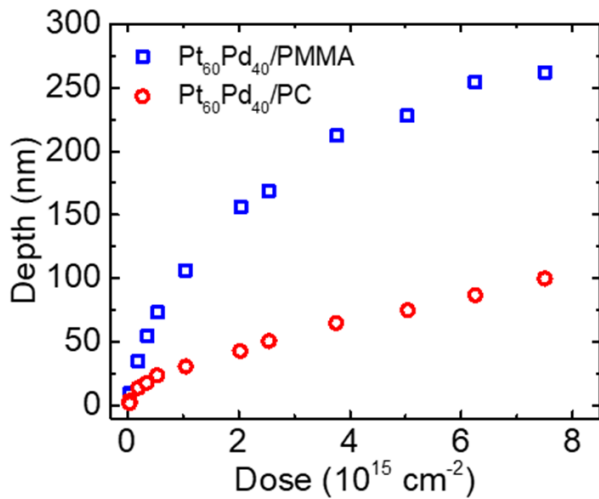


**Figure 6:** Dose dependence of the irradiation induced depth for the Pt<sub>60</sub>Pd<sub>40</sub> / PC sample. For comparison, the dose dependence for a 15nm Pt<sub>60</sub>Pd<sub>40</sub> / 770 nm PMMA sample measured in our previous study [4] is also presented. The samples were irradiated with a 25 keV He<sup>+</sup> FIB within a dose range from  $4.0 \times 10^{13}$  to  $7.5 \times 10^{15} \text{ cm}^{-2}$ .

### Irradiation of PDMS

In terms of surface morphology and its dependence on the irradiation dose, the results obtained for the PDMS samples appeared to be profoundly different from the results obtained for the PMMA and PC samples. Figure 7 shows examples of He<sup>+</sup> ion irradiation of 15 nm Pt<sub>60</sub>Pd<sub>40</sub>/PDMS samples using square and circular patterns. Here, the irradiation of the PDMS samples with He<sup>+</sup> FIB results in the formation of complex surface patterns. The patterns are composed of the surface depressions in the irradiated areas and surface ripples surrounding the irradiated areas. The surface depressions are of concave shapes characterized by maximum surface depths at the geometrical centers of the irradiated squares (Figure 7a) and circles (Figure 7b). Some additional features (rectangular shape elevations at the left-hand sides of circles **B2** and **B3** in Figure 7b) are artefacts generated by scanning these areas with the He<sup>+</sup> ion probe beam for imaging just after the irradiation. The dependence of maximum surface sinking depth on ion dose was measured in both arrays and is presented in Figure 8. In contrast to the dose dependence revealed for the PMMA and PC samples, the graphs for the PDMS samples include a region with a negative slope within an intermediate dose range, from about  $3.7 \times 10^{14} \text{ cm}^{-2}$  to  $2.0 \times 10^{15} \text{ cm}^{-2}$ . This means that, while at low and high doses the irradiated material volume pulls the surface down, in the intermediate dose range it pushes the surface back to the baseline position. In other words, with an increase in the irradiation dose, the PDMS material first shrinks, then swells and then again shrinks.

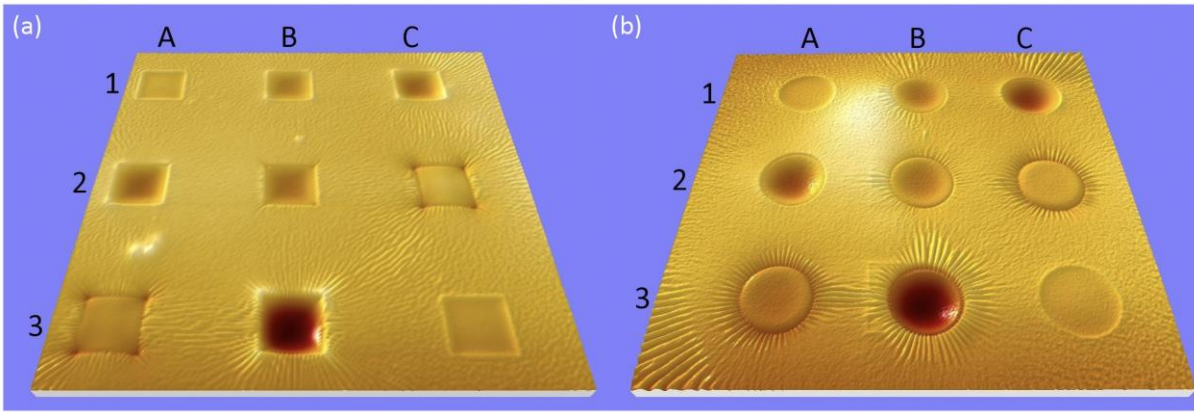


**Figure 7:** HIM images of square (a) and circular (b) arrays produced in 15 nm Pt<sub>60</sub>Pd<sub>40</sub>/PDMS sample by irradiation with different doses of 25 keV-He<sup>+</sup> ions. In both images, the irradiation dose increases in a raster scan order as follows: **A1** ( $3.7 \times 10^{13} \text{ cm}^{-2}$ ), **B1** ( $2.0 \times 10^{14} \text{ cm}^{-2}$ ), **C1** ( $3.7 \times 10^{14} \text{ cm}^{-2}$ ), **A2** ( $5.3 \times 10^{14} \text{ cm}^{-2}$ ), **B2** ( $1.0 \times 10^{15} \text{ cm}^{-2}$ ), **C2** ( $2.0 \times 10^{15} \text{ cm}^{-2}$ ), **A3** ( $2.5 \times 10^{15} \text{ cm}^{-2}$ ), **B3** ( $5.0 \times 10^{15} \text{ cm}^{-2}$ ), **C3** ( $3.7 \times 10^{13} \text{ cm}^{-2}$ ). The lowest dose was irradiated in two cells (**A1** and **C3**) to control the reproducibility of the obtained results. The length of the square side and of the circle diameter is 10  $\mu\text{m}$ .

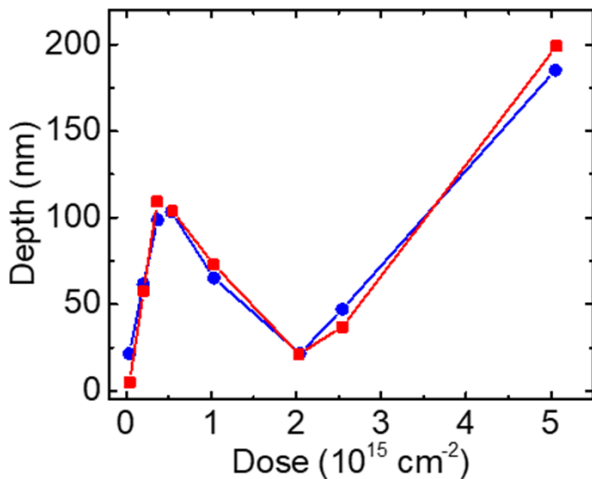


**Figure 8:** Dose dependence of the irradiation induced depth for a 15 nm Pt<sub>60</sub>Pd<sub>40</sub>/PDMS sample irradiated with a 25 keV He<sup>+</sup> FIB within a dose range from  $3.7 \times 10^{13}$  to  $5.0 \times 10^{15} \text{ cm}^{-2}$ . The depth is determined as the maximum depth within each irradiated area. Red squares and blue circles correspond to measurements performed in the irradiated areas of Fig.7a and Fig.7b, respectively.

The concave shapes of the surface inside the irradiated PDMS regions can to a large extent be attributed to the elasticity of this material. A very low Young's modulus of 1.32 to 2.97 MPa for the Sylgard-184 PDMS material [28] provides relaxation of mechanical strain on much larger distances as compared to a short-range strain relaxation in non-elastic polymers such as PPMMA and PC. Therefore, instead of directly projecting the initially flat surface to another depth position, the irradiation-induced strain warps the pristine surface shape. The existence of the long-range strain fields,

sufficient for the significant surface deformation in our PDMS samples, is indicated by the observation of ripple patterns around the irradiated areas. Other features associated with the strain fields in highly elastic materials are the sharp surface elevations or depressions at the corners of the irradiated squares in Figure 7b. From a continuum mechanics point of view, these features are places for stress concentration, resulting in enhancement of the local deformations.

Note that in numerous previous studies the occurrence of the ripples (also referred to in the literature as ‘wrinkles’) on the irradiated PDMS surface has been reported. It is attributed to the formation of a silica-like, stiff skin-layer that buckles to release the accumulated strain energy (see e.g. Ref. [29]). Remarkably, we did not observe any rippling in the irradiated areas, in the entire dose range. The only ripple patterns we observed are those generated by the stress field outside the irradiated regions, where there is no skin or other structural or compositional material modification. One of the likely reasons for the absence of rippling inside the irradiated areas is that the density of the total energy lost by  $\text{He}^+$  ions in our PDMS samples is not large enough to build-in sufficiently high stress to trigger rippling. This result is also interesting from the point of view of potential applications, because it opens up for a possibility of changing surface curvature on the microscale scale while preserving surface nanomorphology.

An even more remarkable result is the transition, from shrinkage to expansion and then from expansion to shrinkage, as a function of the irradiation dose (Figure 8). To explain this non-trivial surface kinetics, we assume that the structural transformations in the irradiated PDMS material depend on the mechanical strain induced in the irradiated polymer volume by the compacting process. In this case, the strain accumulates with the irradiation dose, and at certain dose, reaches a threshold level resulting in changes in the structural reconstruction processes, that leads to the transition from a compacting to an expansion phase. We emphasize that such a transition is favorable from a thermodynamic point of view because volume expansion provides relaxation of tensile strain specific to the compacted regions and therefore results in reduction in strain energy accumulated in the system. The energy minimization provides a thermodynamic force for the strain relaxation, but in addition to this, kinetic means are required to carry out the relaxation process. As a matter of fact, the kinetic means in the present case are provided by ion irradiation in a form of scissioned atomic bonds, which reduce energy barriers for material expansion. This entirely phenomenological model is consistent with the conclusions of work [25], where swelling was observed in PDMS samples irradiated with a 2 MeV proton beam, in the case that the irradiated surface was a cut surface fabricated by cutting a piece of the PDMS polymer out a bulk sample. In contrast, the irradiation of a pristine PDMS surface of this sample resulted in material compacting. The authors explained this difference by mechanical stress in the cut surface.

Other important aspects of the PDMS material transformation induced by ion irradiation include irreversible changes in material structure and elastic properties with an increase in the irradiation dose [21-25]. These factors can contribute significantly in setting the threshold dose for the first, strain-driven, transition and can be responsible for the occurrence of

the second transition followed by material shrinking in the high dose range. We also do not exclude that a certain accumulation of radiolysis gases inside the irradiated volume occurs in our samples, and to some degree can contribute to shaping the depth-vs-dose dependencies presented in Figure 8. Obviously, further structural studies are required to elaborate on the factual contributions of the radiation effects and material parameters.

We emphasize that the suggested method for controlling the out-plane position of surface features can be interesting for fabrication of a range of micro-optical and microfluidic devices and micro-electromechanical systems (MEMS). Possible applications for the micro-optical devices are discussed in detail in our previous work [4], and include tuning the thickness of the dielectric layer in metal-insulator-metal (MIM) structures used in linearly variable bandpass filters (LVBFs) [30-33]. The capabilities of PDMS substrates for multiscale surface curving are also very interesting from the point of view of manufacturing photonic structures and micro-lens arrays. Nanometer-thick gaps and cavities with the prefabricated nanostructures can be implemented in different schemes for nanoparticle control and separation in microfluidic systems [34], and as components of actuators or switches in MEMS [35, 36].

## Conclusions

In conclusion, a new technique for the out-of-plane patterning of nanostructures prefabricated on the surface of polymer substrates has been investigated. The technique is based on ion-beam-induced material modification in the bulk of an underlying polymer substrate and provides surface manipulation while sustaining the prefabricated surface nanofeatures. The role of the subsurface and surface processes in the modification of the surface morphology has been studied for three types of polymers (PMMA, PC and PDMS) by using exposures to  $\text{He}^+$ ,  $\text{Ne}^+$  and  $\text{Ga}^+$  focused ion beams in a Zeiss Orion NanoFab Helium Ion Microscope. Thin metal films of an  $\text{Pt}_{60}\text{Pd}_{40}$ -alloy and of pristine Au were used for modeling the prefabricated nanostructures. We show that the surface height of the thin  $\text{Pt}_{60}\text{Pd}_{40}$  film deposited on PMMA and PC polymer substrates can be patterned by  $\text{He}^+$  ion beam with nanometer precision, while preserving significant features of the pre-deposited film. The irradiation of Au-coated samples results in delamination of the Au thin film followed by its bulging and perforation which points to the important role of availability of pathways for desorption of radiolysis gases. The irradiation with  $\text{Ne}^+$  or  $\text{Ga}^+$  ion beams destroys the films and roughens the surface due to prevalence of a high-ion-mass induced sputtering process. Very different ion-irradiation effects, such as formation of complex, multiscale surface patterns, and a transition from polymer compacting to polymer swelling were observed in the coated and irradiated PDMS samples. The roles of the prefabricated film structure, elastic properties of the polymer substrates and mechanical strain in the patterning process are elaborated and discussed.

## Experimental procedures

## Materials and samples

The PMMA and PDMS substrates used in this study were deposited on the surface of blank silicon wafers. The deposition of PMMA was performed by spin-coating technique in an RRT Lanz EBS 11 spin-coater. The material and deposition parameters are presented in Table S1 of the supplementary material. After the deposition, samples were annealed at 200 °C for 90 s to remove solvent residuals. The PDMS polymer was a two-component, Dow Sylgard™184 silicone elastomer with a hardness value of 43 in the Durometer Shore scale. After mixing the components, the elastomer was dispensed on the surface of the silicon wafer, degassed in vacuum and cured for 48 hours at room temperature, which resulted in the formation of an about 0.8 mm thick PDMS layer. For the preparation of PDMS samples we intentionally avoided any spin-coating, in order to fabricate a uniform layer that is free from any spinning-induced structural anisotropy [37]. The PC samples were 10 x 10 mm<sup>2</sup> square pieces cut from 1.5 mm thick wafers of an optical-grade PC polymer manufactured by microfluidic ChipShop GmbH.

Thin metal films of either an Pt<sub>60</sub>Pd<sub>40</sub> alloy or Au were deposited on the surface of the polymer substrates to study patterning these films by in-bulk processes. An important argument for using metal films is that these films avoid surface charging, and therefore, use of charge compensation by irradiation with electron beams, which can generate additional radiation damage in polymer materials. The Pt<sub>60</sub>Pd<sub>40</sub> alloy films were deposited by DC sputtering in a Cressington 208HR sputter apparatus. The Au films were deposited with e-beam in a Cryofox Explorer 600 physical vapor deposition system. We have been using very thin metal films (5 and 15 nm thick) to minimize the ion path length in these films, and therefore potential sputtering effects.

## FIB Irradiation and sample characterization

The irradiation of the samples with He<sup>+</sup>, Ne<sup>+</sup> and Ga<sup>+</sup> ions was done in a Zeiss Orion NanoFab Helium Ion Microscope at a landing energy of 25 keV and with doses in the range between  $1.0 \times 10^{13}$  cm<sup>-2</sup> to  $2.0 \times 10^{16}$  cm<sup>-2</sup>. The beam current was kept at a value of around 1.7 pA for all irradiations with He<sup>+</sup> and Ne<sup>+</sup> ions, and around 2.0 pA for irradiations with Ga<sup>+</sup> ions. A beam dwell time of 2 μs was used for all irradiations. Arrays of 10 x 10 μm<sup>2</sup> squares irradiated with different doses were used for measurements of the surface height dependence on the irradiation dose, as described in Ref. [4]. The distance between the edges of squares was kept either 10 μm or 15 μm to avoid possible interactions between the irradiated areas, such as for instance overlaps originating from the transverse ion straggle.

The samples were characterized with atomic force microscopy (AFM) and Helium ion microscopy (HIM). The measurements of the surface height were performed with a Veeco Dimension 3100 AFM instrument in the tapping mode.

High-resolution imaging by He<sup>+</sup> ion-beam probe was done with a very small beam current (below 0.1 pA) to minimize imaging artefacts from radiation damage generated by the probe beam.

## Acknowledgements

Partfunding from Interreg Deutschland-Danmark within the European Regional Development Fund (ERDF) via the CELLTOM project is gratefully acknowledged.

## Supplementary material

### I) Sample preparation

**Table S1:** Spin-coating parameters used for the deposition of PMMA layers

Material	950 PMMA A4
1st step	1000 rpm for 5 s, 1500 rpm/s
2nd step	7000 rpm for 45 s, 10000 rpm/s
Layer thickness	200 nm

## II) SRIM simulations

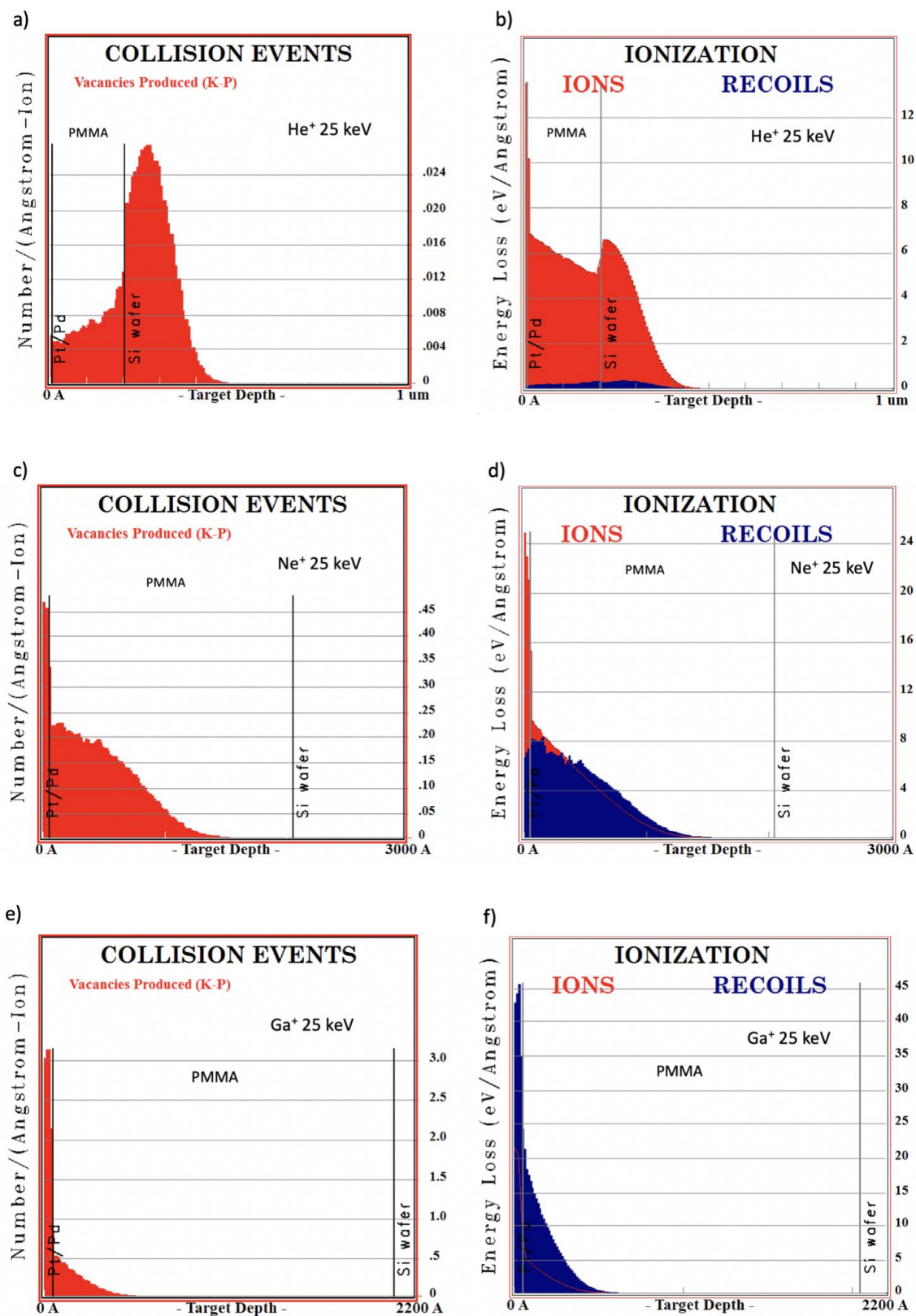


**Figure S1:** SRIM simulations of collision and ionization in the 5 nm Pt<sub>60</sub>Pd<sub>40</sub>/200 nm PMMA samples, irradiated with He<sup>+</sup> ((a) and (b)), Ne<sup>+</sup> ((c) and (d)), and Ga<sup>+</sup> ((e) and (f)) FIBs.

## References

- 1) Yao, N., Ed. *Focused Ion Beam Systems: Basics and Applications*; Cambridge University Press: Cambridge, U.K., 2007.
- 2) Joy, D. C. *Helium Ion Microscopy - Principles and Applications*; 1st ed.; Springer: New York, U.S.A., 2013.
- 3) Shorubalko, I.; Pillatsch, L.; Utke, I. Direct-Write Milling and Deposition with Noble Gases. In *Helium Ion Microscopy*; Hlawacek, G.; Götzhäuser, A., Eds.; Springer International Publishing: Switzerland, 2016; pp 355-393.
- 4) Tavares, L.; Chiriaev, S.; Adashkevich, V.; Taboryski, R.; Rubahn, H-G. *Nanotechnology* **2020**, *31*, 145303.
- 5) Kondyurin, A.; Bilek, M. *Ion Beam Treatment of Polymers - Application aspects from medicine to space*, 2nd ed.; Elsevier: Amsterdam, 2014.
- 6) Zhang, L.; Thomas, J. P.; Guan, X.; Heinig, N. F.; Leung, K. T. *Nanotechnology* **2020**, *31*, 325301
- 7) Thomaz, R. S.; Papaléo, R. M. Ion Beam Modification of Poly (methyl methacrylate) (PMMA). In *Radiation Effects in Polymeric Materials*; Kumar, V.; Chaudhary, B.; Sharma, V.; Verma, K., Eds.; Springer Nature Switzerland AG: Switzerland, 2019; pp 112-137.
- 8) Haiducu, M.; Rahbar, M.; Foulds, I. G.; Johnstone, R. W.; Sameoto, D.; Parameswaran, M. *J. Micromech. Microeng.* **2008**, *18*, 115029.
- 9) Valiev, K. A. *The Physics of Submicron Lithography*, 1st ed.; Springer US: New Yourk, U.S.A.,1992.
- 10) Licciardello, A.; Fragalà, M. E.; Foti, G.; Compagnini, G.; Puglisi, O. *Nucl. Instr. and Meth. in Phys. Res.* **1996**, *B 116*, 168-172.
- 11) Schrepel, F.; Kim, Y. S.; Witthuhn, W. *Appl. Surf. Sci.* **2002**, *189*, 102-112.
- 12) Torrisi, L. *Radiation Effects and Defects in Solids* **1998**, *145*, 285-296.
- 13) Koval, Y. *J. Vac. Sci. Technol.* **2004**, *B 22*, 843-851.
- 14) Olabisi, O.; Adewale, K. Eds. *Handbook of Thermoplastics*, 2nd ed.; CRC Press: U.S.A., 2016.
- 15) Abbas, A. S.; Yavuz, M.; Cui, B. *Microelectronic Engineering* **2014**, *113*, 140–142.
- 16) Apel, P. *Radiation Meas.* **2001**, *34*, 559–566.
- 17) Zheng, N.; Min, H.; Jiang, Y.; Cheng, X. *J. Vac. Sci. Technol.* **2018**, *B 36*, 021603.
- 18) Toimil Molares, M. E.; Brötz, J.; Buschmann, V.; Dobrev, D.; Neumann, R.; Scholz, R.; Schuchert, I. U.; Trautmann, C.; Vetter, J. *Nucl. Instr. Meth. Phys. Res.* **2001**, *B 185*, 192–197.
- 19) Mark, J. E., Ed. *Physical Properties of polymers handbook*, 2nd ed.; Springer Science + Business Media: U.S.A., 2007.
- 20) Tiwari, A.; Soucek, M. D. Eds. *Concise Encyclopedia of High Performance Silicones*; John Wiley & Sons, Inc.: Hoboken, NJ, U.S.A., 2014.

- 21) Huszank, R. Irradiation Induced Chemical and Physical Effects in Silicones. In *Concise Encyclopedia of High Performance Silicones*; Tiwari, A.; M. D. Soucek, M. D., Eds.; John Wiley & Sons, Inc., Hoboken, NJ, U.S.A., 2014; pp 75-84.
- 22) Huszank, R.; Bonyár, A.; Kámán, J.; Furu, E. *Polymer Degradation and Stability* **2018**, *152*, 253-258.
- 23) Moon, M. W.; Lee, S. H.; Sun, J. Y.; Oh, K. H.; Vaziri, A.; Hutchinson, J. W. *Proc. Natl. Acad. Sci.* **2007**, *104*, 1130-1133.
- 24) Lee, S.; Yang, J.; Jung, S.; Kim, D-G.; Byeon, E. *Appl. Sci. Conver. Technol.* **2018**, *27*, 130-134.
- 25) Szilasi, S. Z.; Huszank, R.; Csik, A.; Cserháti, C.; Rajta, I. *Nucl. Instrum. and Meth. in Phys. Res.* **2009**, *B 267*, 2296–2298.
- 26) Hareesh, K.; Sanjeev, G. Effects of Radiations on the Properties of Polycarbonate. In *Radiation Effects in Polymeric Materials*; Kumar, V.; Chaudhary, B.; Sharma, V.; Verma, K., Eds.; Springer Nature Switzerland AG: Switzerland, 2019; pp 293-318.
- 27) Thorat, A. B.; Sonawane, A.; Jadhav, A.; Dhole, S. D.; Dahiwalea, S. S. Effect of low energy Ar<sup>+</sup> ion irradiation on polycarbonate. In *AIP Conference Proceedings* **2019**, *2115*, 030328.
- 28) Johnston, I. D.; McCluskey, D. K.; Tan, C. K. L.; Tracey, M. C. *J. Micromech. Microeng.* **2014**, *24*, 035017.
- 29) Winton, B. R.; Ionescu, M.; Dou, S. X.; Wexler, D.; Alvarez, G. A. *Acta Materialia* **2010**, *58*, 1861-1867.
- 30) Emadi, A.; Wu, H.; De Graaf, G.; Hedsten, K.; Enoksson, P.; Correia, J. H.; Wolffenbuttel, R. F. *Procedia Engineering* **2010**, *5*, 416–419.
- 31) Williams, C.; Rughoobur; G.; Flewitt, A. J.; Wilkinson, T. D. *Appl Opt.* **2016**, *55*, 9237-9241.
- 32) Li, Z.; Butun, S.; Aydin, K.; *ACS Photonics* **2015**, *2*, 183– 188.
- 33) Grushina, A. *Adv. Opt. Technol.* **2019**, *8*, 163-169.
- 34) Salafi, T.; Zeming, K. K.; Zhang, Y. *Lab Chip* **2017**, *17*, 11-33.
- 35) Sugiyama, S.; Amaya, S.; Dao, D. V. *Adv. Nat. Sci.: Nanosci. Nanotechnol.* **2012**, *3*, 015009.
- 36) Wang, K.; Ouyang, G.; Chen, X.; Jakobsen, H. *Polymer Reviews* **2017**, *57*, 369-396.
- 37) Liu, M.; Sun, J.; Sun, Y.; Christopher Bock, C.; Chen, Q. *J. Micromech. Microeng.* **2009**, *19*, 035028.